

# A digital SRAM-based compute-in-memory macro for weight-stationary dynamic matrix multiplication in Transformer attention score computation

Jianyi Yu

School of Microelectronics and Communication Engineering, Chongqing University, 400030 Chongqing, China  
[jianyiyu@cqu.edu.cn](mailto:jianyiyu@cqu.edu.cn)

Tengxiao Wang

School of Microelectronics and Communication Engineering, Chongqing University, 400030 Chongqing, China  
[tengxiao.wang@stu.cqu.edu.cn](mailto:tengxiao.wang@stu.cqu.edu.cn)

Yuxuan Wang

School of Microelectronics and Communication Engineering, Chongqing University, 400030 Chongqing, China  
[202312131166@stu.cqu.edu.cn](mailto:202312131166@stu.cqu.edu.cn)

Xiang Fu

School of Microelectronics and Communication Engineering, Chongqing University, 400030 Chongqing, China  
[fuxiang@cqu.edu.cn](mailto:fuxiang@cqu.edu.cn)

Ying Wang

Institute of Computing Technology, Chinese Academy of Sciences, 100190 Beijing, China  
[wangying2009@ict.ac.cn](mailto:wangying2009@ict.ac.cn)

Fei Qiao

Department of Electronic Engineering, Tsinghua University, 100084 Beijing, China  
[qiaofei@tsinghua.edu.cn](mailto:qiaofei@tsinghua.edu.cn)

Liyuan Liu

Institute of Semiconductors, Chinese Academy of Sciences, 100083 Beijing, China,  
[liuly@semi.ac.cn](mailto:liuly@semi.ac.cn)

Cong Shi\*

School of Microelectronics and Communication Engineering, Chongqing University, 400030 Chongqing, China  
[shicong@cqu.edu.cn](mailto:shicong@cqu.edu.cn)

\*Corresponding author

**Abstract**—Compute-in-memory (CIM) techniques are widely employed in energy-efficient artificial intelligent (AI) processors. They alleviate power and latency bottlenecks caused by extensive data movements between compute and storage units. This work proposes a digital CIM macro to compute Transformer attention. To mitigate dynamic matrix multiplication that is unsuitable for the common weight-stationary CIM paradigm, we reformulate the attention score computation process based on a combined QK-weight matrix, so that inputs can be directly fed to CIM cells to obtain the score results. Moreover, the involved binomial matrix multiplication operation is decomposed into 4 groups of bit-serial shifting and additions, without costly physical multipliers in the CIM. We maximize the energy efficiency of the CIM circuit through zero-value bit-skipping, data-driven word line activation, read-write separate 6T cells and bit-alternating 14T/28T adders. The proposed CIM macro was implemented using a 65-nm process. It occupied only 0.35 mm<sup>2</sup> area, and delivered a 42.27 GOPS peak performance with 1.24 mW power consumption at a 1.0 V power supply and a 100 MHz clock frequency, resulting in 34.1 TOPS/W energy efficiency and 120.77 GOPS/mm<sup>2</sup> area efficiency. When compared to the CPU and GPU, our CIM macro is  $\sim 25\times$  and  $\sim 13\times$  more energy efficient on practical tasks, respectively. Compared with other Transformer-CIMs, our design exhibits at least 7 $\times$  energy efficiency and at least 2 $\times$  area efficiency improvements when scaled to the same technology node, showcasing its potential for edge-side intelligent applications.

**Keywords**—Transformer, attention, compute-in-memory, CIM, energy-efficient

## I. INTRODUCTION

The emergence of the Transformer has driven significant advancements in the AI fields, attracting considerable research interest. This success stems from both algorithmic innovation and the rapid improvement of hardware capabilities. However, the huge computational loads of Transformers are outpacing the

improvement of current hardware performance. Furthermore, the intensive data movement between computation and memory units during training and inference exacerbates the traditional von Neumann architecture’s “memory wall” bottleneck. To overcome this challenge, researchers are exploring compute-in-memory (CIM) [1], [2] techniques, shifting from a compute-centric to a data-centric approach to minimize data transfer. By integrating multiply-accumulate (MAC) function into memory array, the primary advantage of CIM lies in its energy-efficient matrix multiplication (MM) for neural network and Transformer models [3].

However, the Transformer’s attention mechanism presents novel memory access challenges for CIM designs. Traditional neural networks and the fully connected layers within Transformers rely on static MM, where the weights remain constant throughout inference. CIM [4], [5] can store these weights once and reuse them efficiently. However, the attention mechanism uses dynamic MM (e.g.,  $Q \times K^T$ ), where  $Q$  and  $K$  are dynamically generated. This requires CIM to repeatedly store and access this dynamic data, causing redundant memory access and increased power consumption and latency. Moreover, the generation direction of  $K$  mismatches the CIM write direction, needing an extra transpose buffer. Thus, redesigning CIM is essential to handle dynamic MM efficiently in Transformers.

In this context, many researchers are actively researching the application of CIM technology in Transformers. TranCIM [6] aims to eliminate redundant memory access for  $Q$  and  $K$  by implementing partial pipelining. However, it requires a large global buffer for pipeline segmentation. To address the global buffer issue caused by TranCIM and further eliminate redundant memory access, P<sup>3</sup>ViT [7] proposed three pipeline scheduling modes to optimize memory access. Concurrently, CIMFormer [8] introduces a token pruning-based attention mechanism that

avoids computing less important tokens, thereby reducing memory access in CIM. The researches primarily leverage the benefits of pipelined architectures, leading to significant improvements in overall performance and computational efficiency. However, it inevitably incurs overhead due to buffering intermediate data and introduces complex pipeline control circuits. AttCIM [9] utilizes a ring-shaped CIM architecture to perform dynamic MM involving  $\mathbf{Q}$  and  $\mathbf{K}$  through matrix decomposition. This approach eliminates the need to load dynamically generated matrices into the CIM macro. Yet, AttCIM introduces a new overhead for memory access when storing the input matrices  $\mathbf{X}$  in CIM.

To address the power consumption and latency caused by redundant memory access in the above Transformer-CIMs, this work proposes a digital CIM macro for energy-efficiency computation in Transformer attention. The main contributions of this work include:

(1) In Section II, we reformulate the attention score computation process based on a combined QK-weight matrix to mitigate dynamic matrix multiplication. This enables direct input to CIM cells to obtain score results. Moreover, we decompose the binomial matrix multiplication into four groups of bit-serial shifting and additions, avoiding the need for costly physical multipliers in the CIM.

(2) In Section III, we maximize the energy efficiency of the CIM circuit through zero-value bit-skipping, data-driven word line activation, read-write separate 6T cells and bit-alternating 14T/28T adders.

(3) In Section IV, We implemented this energy-efficient and scalable CIM macro in 65-nm technology and conducted extensive experiments to validate its performance across multiple aspects.

## II. ALGORITHM MODEL

### A. Pre-calculation of $\mathbf{W}_K$ and $\mathbf{W}_Q$ Multiplication

In the traditional Transformer, the calculation of the attention score matrix  $\mathbf{S}$  in the attention mechanism is presented in Eq. (1):

$$\mathbf{S} = \mathbf{Q}\mathbf{K}^T = \mathbf{X}\mathbf{W}_Q(\mathbf{X}\mathbf{W}_K)^T = \mathbf{X}\mathbf{W}_Q\mathbf{W}_K^T\mathbf{X}^T \quad (1)$$

Where  $\mathbf{S} \in \mathbb{R}^{N \times N}$  is the Attention Map,  $\mathbf{Q} \in \mathbb{R}^{N \times d}$  is the query matrix,  $\mathbf{K} \in \mathbb{R}^{N \times d}$  is the key matrix, and  $\mathbf{X} \in \mathbb{R}^{N \times d_{\text{model}}}$  is the input matrix composed of  $N$  tokens, each with a dimension of  $d_{\text{model}}$ .  $\mathbf{W}_Q$  and  $\mathbf{W}_K \in \mathbb{R}^{D \times d}$  are the corresponding weight matrices. However,  $\mathbf{Q}$  and  $\mathbf{K}$  in Eq. (1) are generated dynamically. The required dynamic MM is unsuitable for the common weight-stationary CIM paradigm.

In Transformer inference,  $\mathbf{W}_Q$  and  $\mathbf{W}_K$  from Eq. (1) are constant. Therefore, changes in the output are solely determined by  $\mathbf{X}$ . As shown in Fig. 1(a), we pre-compute the matrix product of  $\mathbf{W}_Q$  and  $\mathbf{W}_K$ , resulting in a new weight matrix  $\mathbf{W}_{QK}$ :

$$\mathbf{W}_{QK} = \mathbf{W}_Q\mathbf{W}_K^T \in \mathbb{R}^{D \times D} \quad (2)$$

Subsequently, by substituting Eq. (2) into Eq. (1), we derive the following expression:

$$\mathbf{S} = \mathbf{X}\mathbf{W}_{QK}\mathbf{X}^T \quad (3)$$

To compute the elements of the attention score matrix  $\mathbf{S}$ , the input matrix  $\mathbf{X}$  is flattened by rows as follows:

$$\mathbf{X} = \begin{bmatrix} \mathbf{X}_1 \\ \mathbf{X}_2 \\ \vdots \\ \mathbf{X}_N \end{bmatrix} \quad (4)$$

Thus, the elements of matrix  $\mathbf{S}$  can be arranged as follows:

$$\mathbf{S} = \begin{bmatrix} \mathbf{X}_1\mathbf{W}_{QK}\mathbf{X}_1^T & \mathbf{X}_1\mathbf{W}_{QK}\mathbf{X}_2^T & \cdots & \mathbf{X}_1\mathbf{W}_{QK}\mathbf{X}_N^T \\ \mathbf{X}_2\mathbf{W}_{QK}\mathbf{X}_1^T & \mathbf{X}_2\mathbf{W}_{QK}\mathbf{X}_2^T & \cdots & \mathbf{X}_2\mathbf{W}_{QK}\mathbf{X}_N^T \\ \vdots & \vdots & \ddots & \vdots \\ \mathbf{X}_N\mathbf{W}_{QK}\mathbf{X}_1^T & \mathbf{X}_N\mathbf{W}_{QK}\mathbf{X}_2^T & \cdots & \mathbf{X}_N\mathbf{W}_{QK}\mathbf{X}_N^T \end{bmatrix} \quad (5)$$

Specifically, the element  $s_{ij}$  in the  $i$ -th row and  $j$ -th column of matrix  $\mathbf{S}$  is given by:

$$s_{ij} = \mathbf{X}_i\mathbf{W}_{QK}\mathbf{X}_j^T \quad (6)$$

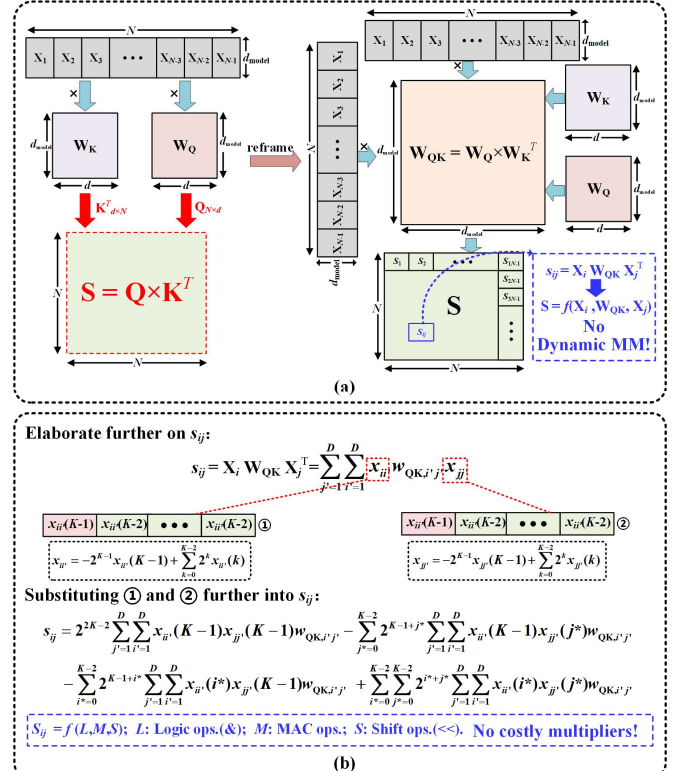


Fig. 1. The process of attention score computation is reformulated for CIM using a combined QK-weight matrix and bit-serial decomposition. (a) The process of

pre-computing  $\mathbf{W}_K$  and  $\mathbf{W}_Q$  Multiplication. (b) The process of bit slicing divides input data into single bits.

Therefore, each element  $s_{ij}$  of the matrix  $\mathbf{S}$  can be directly computed from the pre-computed weight matrix  $\mathbf{W}_{QK}$  and the corresponding input vectors  $\mathbf{X}_i$  and  $\mathbf{X}_j$ .

### B. Bit-Slicing Technology for Input Data

As shown in Fig. 1(b), we further expand Eq. (6) to derive the following computational expression for  $s_{ij}$ :

$$s_{ij} = \sum_{i'=1}^D \sum_{j'=1}^D x_{ii'} w_{QK,i'j'} x_{jj'} \quad (7)$$

Where  $x_{ii'}$  represents the  $i'$ -th component of the row vector  $\mathbf{X}_i$ ,  $x_{jj'}$  represents the  $j'$ -th component of the column vector  $\mathbf{X}_j$ , and  $w_{QK,i'j'}$  represents the element in the  $i'$ -th row and  $j'$ -th column of matrix  $\mathbf{W}_{QK}$ . It is important to note that the indices  $i$  and  $i'$ , and the indices  $j$  and  $j'$ , are mutually independent.

To implement CIM, we must express  $x_{ii'}$  and  $x_{jj'}$  in terms of their binary representations. Thus, we further expand:

$$x_{ii'} = -2^{K-1} x_{ii'}(K-1) + \sum_{k=0}^{K-2} 2^k x_{ii'}(k) \quad (8)$$

$$x_{jj'} = -2^{K-1} x_{jj'}(K-1) + \sum_{k=0}^{K-2} 2^k x_{jj'}(k) \quad (9)$$

Where  $K$  represents the bit width of  $x_{ii'}$  and  $x_{jj'}$ , with the most significant bit serving as the sign bit. Substituting Eq. (8) and Eq. (9) into Eq. (7), we can obtain:

$$\begin{aligned} s_{ij} &= \sum_{j'=0}^D \sum_{i'=1}^D (-2^{K-1} x_{ii'}(K-1) + \sum_{i=0}^{K-2} 2^i x_{ii'}(i^*)) w_{QK,i'j'} (-2^{K-1} x_{jj'}(K-1) + \sum_{j=0}^{K-2} 2^j x_{jj'}(j^*)) \\ &= 2^{2K-2} \sum_{j'=0}^D \sum_{i'=1}^D x_{ii'}(K-1) x_{jj'}(K-1) w_{QK,i'j'} \\ &\quad - \sum_{j^*=0}^{K-2} 2^{K-1+j^*} \sum_{j'=1}^D \sum_{i'=1}^D x_{ii'}(K-1) x_{jj'}(j^*) w_{QK,i'j'} \\ &\quad - \sum_{i^*=0}^{K-2} 2^{K-1+i^*} \sum_{j'=1}^D \sum_{i'=1}^D x_{ii'}(i^*) x_{jj'}(K-1) w_{QK,i'j'} \\ &\quad + \sum_{i^*=0}^{K-2} \sum_{j^*=0}^{K-2+i^*} \sum_{j'=1}^D \sum_{i'=1}^D x_{ii'}(i^*) x_{jj'}(j^*) w_{QK,i'j'} \end{aligned} \quad (10)$$

Where  $x_{ii'}(i^*)$  denotes the  $i^*$ -th bit of the scalar  $x_{ii'}$ , and  $x_{jj'}(j^*)$  denotes the  $j^*$ -th bit of the scalar  $x_{jj'}$ , with  $i^*, j^* = 0, 1, 2, \dots, K-1$ .

Therefore, using Eq. (10) simplifies the computation of the attention score matrix  $\mathbf{S}$ . Specifically, the involved binomial matrix multiplication operation is decomposed into 4 groups of bit-serial shifting and additions, without costly physical multipliers in the CIM macro. Furthermore, this transformation conforms more closely to the design requirements of traditional CIM and effectively avoids the memory access overhead

associated with other Transformer-CIM architectures. Moreover, this transformation further simplifies the control logic, enhancing the overall efficiency of the system.

### III. HARDWARE DESIGN

By reformulating the attention score computation, we implement Eq. (10) in hardware with two modules: CIM and near-memory computing. The CIM bank focuses on the core MAC operations shared by the four groups, while the near-memory computing module concurrently processes more complex functions like intra-groups shifts and inter-groups additions/subtractions. This hardware mapping scheme fully utilizes the CIM's advantages for large-scale parallel MAC operations. At the same time, it effectively reduces the resource overhead from complex logical operations. As a result, overall computational efficiency is boosted. As shown in Fig. 2, the CIM bank includes read-write separated 6T-SRAM array, data-driven word line unit, and CIM accumulator. Furthermore, considering the sparsity commonly present in Transformer input data (the presence of a large number of bit positions with zero-value in multi-bit data), we deeply integrate zero-value bit-skipping mechanism into the input buffer module to achieve efficient computation.

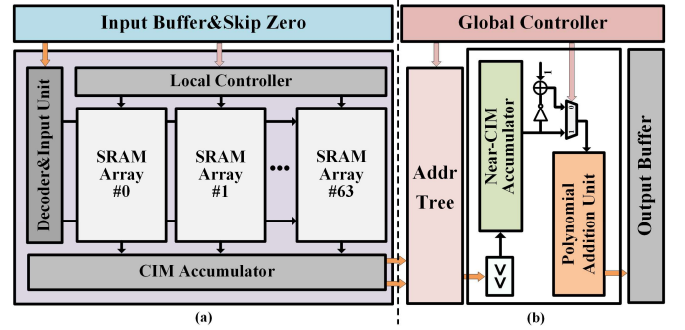


Fig. 2. The proposed CIM macro's overall architecture. (a) The high-performance and scalable CIM bank. (b) The near-memory computing module.

#### A. High-Performance and Scalable CIM bank

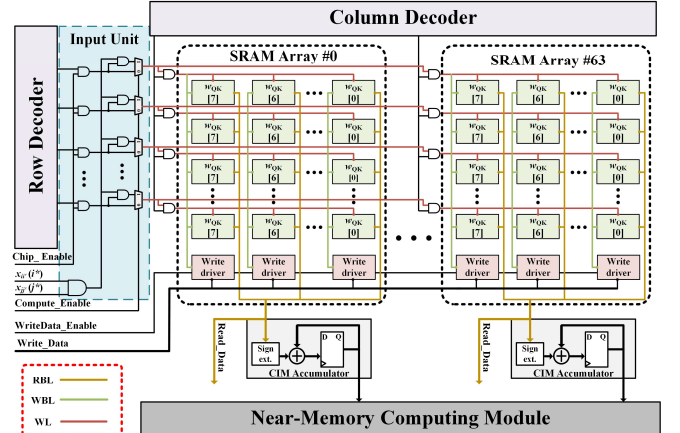


Fig. 3. The high-performance and scalable CIM bank.

As shown in Fig. 3, there are common computations in the four groups of Eq. (10):

$$\sum_{j'=1}^D \sum_{i'=1}^D x_{ii'}(i^*) x_{jj'}(j^*) w_{QK,i'j'} \quad (11)$$

Thus, the single universal CIM bank can execute the operations of Eq. (10). The hardware for the fourth group, which has the highest complexity and universal structure, is mapped first. In the SRAM array, the row data of the weight matrix  $\mathbf{W}_{QK}$  is stored in the row memory units of the array, while the column data is stored in the column memory units. The multiplication operation  $x_{ii'}(i^*) x_{jj'}(j^*) w_{QK,i'j'}$  involves two main steps. First, the “AND” operation is performed on  $x_{ii'}(i^*)$  and  $x_{jj'}(j^*)$ . The result then drives the word line controller, which activates or deactivates the word lines to complete the multiplication with  $w_{QK,i'j'}$ . The multiplication results are then fed into the CIM accumulator and are continuously accumulated over multiple cycles until all input data has been processed.

To compute the complete element  $s_{ij}$ , the calculations for the first three polynomial need to be repeated. Next, the near-memory computing module performs the addition and subtraction of polynomials to obtain the element  $s_{ij}$  in the  $i$ -th row and  $j$ -th column of the attention score matrix  $\mathbf{S}$ . To generate the complete attention score matrix  $\mathbf{S}$ , we still need to iterate through the entire matrix by repeating the above operations until all elements have been computed.

To compute the element  $s_{ij}$ , the near-memory computing module must also complete intra-group shifting and accumulation. It then applies additions and subtractions to the four resulting groups to obtain the element  $s_{ij}$  of the attention score matrix  $\mathbf{S}$ .

### B. Core Computing Unit Circuit

As shown in Fig. 4, the core computing unit of the CIM bank includes read-write separated 6T-SRAM array, data-driven word line unit, and CIM accumulator.

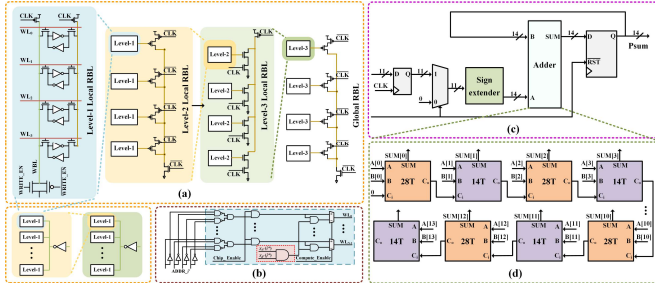


Fig. 4. The core computing unit circuit of the CIM bank. (a) The read-write separated 6T-SRAM array. (b) The data-driven word line unit. (c) The CIM accumulator. (d) The bit-alternating 14T/28T adders.

The read-write separated 6T-SRAM array is designed, as shown in Fig. 4(a). Compared to traditional 8T and 10T structures, this design better meets the core requirements of high integration and energy efficiency in CIM. To solve the read disturbance issue in 6T-SRAM array used in CIM, the 8T-SRAM’s decoupled read design concept was adopted. By separating the write bit line (WBL) from the read bit line (RBL), this approach ensures complete independence between read and write paths, effectively removing voltage disturbances during read operations. To ensure RBL signal integrity in large

memory arrays, a multi-level buffering structure based on NP domino logic was used to process the read bit line.

In the data-driven word line unit in Fig. 4(b), the input signals and word line control function are integrated into the word line driving circuit through the collaboration of a gating logic module and a multiplexer. A three-input “AND” gate is used to merge the input signals and word line control signal, and a multiplexer is used to switch between read/write and compute mode. In compute mode, the input signals activate specific word lines, enabling multiplication between the input signals and the weights. The result is then directly transmitted via the bit lines to the CIM accumulator, thereby completing the accumulation process.

As shown in Fig 4(c), to further reduce power consumption and save area, a high-performance accumulator circuit based on alternating 14T and 28T full adders is implemented. In this work, an alternating data path of 14T and 28T full adders is utilized in Fig. 4(d). The circuit area and power consumption associated with solely using 28T full adders are significantly minimized by this approach, while excessive delay issues that can arise from relying solely on 14T full adders are effectively mitigated.

### C. The Sparsity of Input Data and Zero-Skip Mechanism

In Transformer applications, padding techniques are commonly used to address sequences of varying lengths. By appending zero values to shorter sequences, all input sequences are ensured to be of consistent length, which results in many bits being set to zero in the input tokens. Additionally, the length variations in text sequences lead to short sequences in natural language processing often containing many zero values, while the embeddings of low-frequency words further increase the proportion of these zeros. During the computation of  $x_{ii'}(i^*) x_{jj'}(j^*) w_{QK,i'j'}$ , the presence of any zero bit in the inputs leads to redundant operation, resulting in increased power consumption and latency. To solve this challenge, a zero-value bit-skipping mechanism is integrated into the input buffering module. This mechanism intelligently identifies and bypasses calculations for any zero-value bits present in  $x_{ii'}(i^*)$  and  $x_{jj'}(j^*)$ . By adopting this approach, unnecessary processing cycles are reduced, leading to decreased power consumption and latency. It is indicated by the experimental results that this optimization can reduce power consumption and latency by at least 55% in various applications of the Transformer.

## IV. EVALUATION

Metric	This Work
Technology	65 nm
Macro Area	0.35 mm <sup>2</sup>
Application	Attention
Input	INT8
Weight	INT8
Supply Voltage	1.0 V
Frequency	100 MHz
Power	1.24 mW
Throughput	42.27 GOPS
Energy Efficiency	34.1 TOPS/W
Area Efficiency	120.77 GOPS/mm <sup>2</sup>

Fig. 5. The macro physical layout and specifications.

As shown in Fig. 5, the layout of the digital macro designed for energy-efficient attention computation is presented. The

macro was implemented in a 65-nm process and occupied a total area of 0.35 mm<sup>2</sup>. It had a maximum memory capacity of

TABLE I. COMPARISON WITH THE STATE-OF-THE WORKS

Work	Y. Wang [10] [ISSCC'22]	F. Tu [6] [ISSCC'22]	X. Fu [7] [TCAS-i'23]	S. Liu [12] [ISSCC'23]	R. GUO [9] [JSSC'25]	This work	This work (scaled)
Architecture	No-CIM	Digital CIM	Digital CIM	Digital CIM	Analog CIM	Digital CIM	Digital CIM
Technology (nm)	28	28	28	28	28	65	28
Macro Area (mm <sup>2</sup> )	6.82	6.83	2	3.93	7.09	0.35	0.064 <sup>*4</sup>
Supply Voltage (V)	0.56 - 1.1	0.6 - 1.0	0.6 - 1	0.64 - 1.03	0.56 - 0.9	1.0	0.8
Frequency (MHz)	50 - 510	80 - 240	50 - 200	20 - 320	80 - 275	100	100
Power (mW)	12.06 - 272.8	27.04 - 118.2	20.42-81.83	8.72 - 250.65	43.07 - 57.97	1.24	0.26 <sup>*3</sup>
Peak Performance <sup>*1, 2</sup> (TOPS)	4.07	0.74	0.8	3.33	1.38	0.042	0.042
Energy Efficiency <sup>*1, 2</sup> (TOPS/W)	27.56	20.5	23.24	25.22	19.38	34.09	161.5 <sup>*3</sup>
Area Efficiency <sup>*1, 2</sup> (GOPPS/mm <sup>2</sup> )	596.8	108.3	400	847.3	194.4	120.77	656.25 <sup>*4</sup>

\*1 Off-chip memory access is excluded. All on-chip computing time consumption is included.

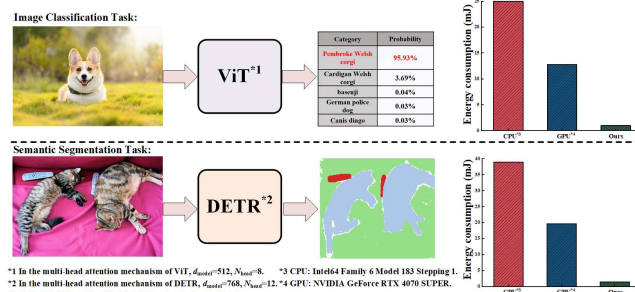
\*2 One operation indicates one addition or multiplication.

\*3 Power scaling from the 65nm to the 28 nm process node is approximately:  $P_{28nm} = P_{65nm} \times (28nm / 65nm) \times (V_{28nm} / V_{65nm})^2 \times (f_{28nm} / f_{65nm})$  [13].

\*4 Area scaling from the 65nm to the 28 nm process node is approximately:  $S_{28nm} = S_{65nm} \times (28nm / 65nm)^2$  [13].

64×64×8 bits for the weights. With a 1 V supply voltage, the macro's power consumption is 1.24 mW. Operating at a frequency of 100 MHz, the macro achieved a peak performance of 42.27 GOPS, a maximum energy efficiency of 34.1 TOPS/W, and an area efficiency of 120.77 GOPS/mm<sup>2</sup>.

#### A. Practical Applications and Performance Comparison



\*1 In the multi-head attention mechanism of ViT,  $d_{model}=512$ ,  $N_{head}=8$ . \*3 CPU: Intel64 Family 6 Model 183 Stepping 1.

\*2 In the multi-head attention mechanism of DETR,  $d_{model}=768$ ,  $N_{head}=12$ . \*4 GPU: NVIDIA GeForce RTX 4070 SUPER.

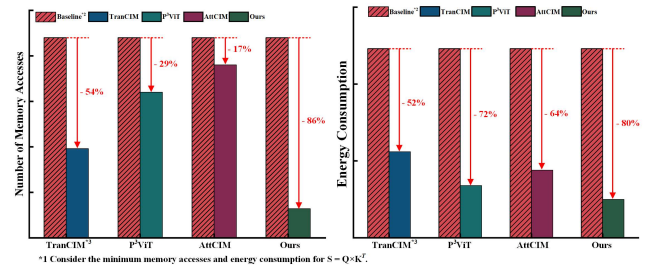
\*5 CPU: Intel64 Family 6 Model 183 Stepping 1, GeForce RTX 4070 SUPER.

Fig. 6. The comparison of the energy efficiency advantage of our work against CPU and GPU for attention score computation.

We implemented a simulation-based approach to evaluate the energy consumption of attention score computation, aiming for a balance of accuracy and efficiency. As a full post-layout simulation of the entire process is too time-consuming, we first created a Verilog behavioral model of our CIM macro. This model allows us to simulate the complete attention score calculation and precisely determine the total operations needed for a specific application. In parallel, we conducted a detailed post-layout simulation on the CIM macro to obtain an accurate energy benchmark for a single operation. The total energy consumption for the application is calculated by the formula: “total operations × single-operation energy benchmark”.

Our experiment involved computing attention scores with the pre-trained ViT and DETR models from the HuggingFace Transformers library. The resulting energy consumption data from the process is shown in Fig. 6. We performed these measurements on a CPU (Intel64 Family 6 Model 183 Stepping 1), a GPU (NVIDIA GeForce RTX 4070), and our CIM macro. The results confirmed our CIM macro's superior energy efficiency. In image recognition, it was 25.2× and 12.9× more efficient than the CPU and GPU, respectively. For visual semantic segmentation, this advantage grew to 26.8× over the CPU and 13.3× over the GPU.

Furthermore, we evaluated several Transformer-CIMs in terms of memory accesses and energy consumption, with the results shown in Fig. 7. The evaluation looked at the least memory accesses needed to compute the attention scores and the lowest energy consumption. The baseline for our comparison was traditional CIM accelerators configured for parallel computation. Our experimental results demonstrated that our approach reduces memory accesses by 6.9× and energy consumption by 4.9× compared to this baseline. Moreover, our CIM macro outperformed other advanced Transformer-CIMs.



\*1 Consider the minimum memory accesses and energy consumption for  $S = Q \times K^2$ .

\*2 Baseline represents traditional CIM accelerators configured for parallel computation, each storing  $W_Q$  and  $W_K$  as 64×64×8-bit weight.

\*3 TranCIM considers only the memory accesses required for CIM computation, without accounting for additional buffers.

Fig. 7. The performance comparison of various Transform-CIM in terms of memory accesses and energy consumption.

### B. Comparison With the State-of-the-Art Works

Table I shows a detailed comparison with the state of-the-art Transformer accelerators. The work in [10] is a digital Transformer accelerator that uses approximate computing techniques for attention. TranCIM [6] and P<sup>3</sup>ViT [7] are digital CIMs with pipelined/parallel reconfigurable mode. A digital CIM with unstructured weight pruning and local attention is proposed in [12]. AttCIM [9] is a digital-assisted CIM array with a CIM ring architecture and data flow reshaping. These works fully leverage the advantages of pipelined structures and the sparsity of data in attention computations to improve energy efficiency.

To ensure a fair comparison, we scaled our work to the 28-nm process node to benchmark against other works. Leveraging the advantages of CIM, our work achieves a 6 $\times$  improvement in energy efficiency compared to [10]. By mitigating the overhead of dynamic matrix multiplication, our work is at least 7 $\times$  more energy-efficient than [6], [7], [9], and [12]. Furthermore, our design demonstrates a significant area advantage, with an area efficiency at least 2 $\times$  higher than that of [6], [7], and [9].

## V. CONCLUSION

This work proposes a digital CIM macro to efficiently accelerate Transformer attention mechanisms. The attention score computation is reformulated through a combined QK-weight matrix. This approach mitigates the dynamic MM in weight-stationary CIM architectures. The binomial MM is decomposed into 4 groups of bit-serial shifting and additions. This avoids costly physical multipliers, boosting efficiency and lowering hardware costs. The CIM circuit's energy efficiency is maximized through a suite of optimizations, including zero-value bit-skipping, data-driven word line activation, read-write separate 6T cells, and bit-alternating 14T/28T adders. Experimental results from the implemented macro validate our approach, showing that our design achieves substantially higher energy efficiency than both CPUs and GPUs on practical workloads. When compared against other state-of-the-art Transformer-CIM accelerators under equivalent conditions, our CIM macro demonstrates significant improvements in both energy and area efficiency. These findings confirm the effectiveness of our methods and highlight the strong potential of this.

## ACKNOWLEDGMENT

This work was funded in part by the Major Research Plan of the National Natural Science Foundation of China under Grant No. 92464103, in part by the Key Program of the National Natural Science Foundation of China under Grant No. 6233400.

## REFERENCES

- [1] Y.-D. Chih et al., “16.4 an 89 TOPS/W and 16.3 TOPS/mm<sup>2</sup> all-digital SRAM-based full-precision compute-in-memory macro in 22 nm for machine-learning edge applications,” in *IEEE Int. Solid-State Circuits Conf. (ISSCC) Dig. Tech. Papers*, pp. 252–254, Feb. 2021.
- [2] X. Si et al., “A local computing cell and 6T SRAM-based computing-in-memory macro with 8-b MAC operation for edge AI chips,” *IEEE J. Solid-State Circuits*, vol. 56, no. 9, pp. 2817–2831, Sep. 2021.
- [3] A. Vaswani et al., “Attention is all you need,” in *Proc. Adv. Neural Inf. Process. Syst.*, pp. 5998–6008, Nov. 2017.
- [4] X. Zhang et al., “A 400 MHz 249.1 TOPS/W 64 Kb fully-reconfigurable SRAM-based digital compute-in-memory macro for accelerating CNNs,” in *Proc. IEEE Asian Solid-State Circuits Conf. (A-SSCC)*, pp. 1–3, Nov. 2023.
- [5] J. Saikia et al., “FP-IMC: A 28 nm all-digital configurable floating-point inmemory computing macro,” in *Proc. IEEE 49th Eur. Solid State Circuits Conf. (ESSCIRC)*, pp. 405–408, Sep. 2023.
- [6] F. Tu et al., “A 28 nm 15.59  $\mu$ J/token full-digital bitline-transpose CIM-based sparse transformer accelerator with pipeline/parallel reconfigurable modes,” in *IEEE Int. Solid-State Circuits Conf. (ISSCC) Dig. Tech. Papers*, pp. 466–468, Feb. 2022.
- [7] X. Fu et al., “P<sup>3</sup>ViT: A CIM-based high-utilization architecture with dynamic pruning and two-way ping-pong macro for vision transformer,” *IEEE Trans. Circuits Syst. I, Reg. Papers*, vol. 70, no. 12, pp. 4938–4948, Dec. 2023.
- [8] R. Guo et al., “CIMFormer: A systolic CIM-array-based transformer accelerator with token-pruning-aware attention reformulating and principal possibility gathering,” *IEEE J. Solid-State Circuits*, vol. 59, no. 10, pp. 3317–3329, Oct. 2024.
- [9] R. Guo et al., “A 28-nm 28.8-TOPS/W Attention-Based NN Processor With Correlative CIM Ring Architecture and Dataflow Reshaped Digital-Assisted CIM Array,” *IEEE J. Solid-State Circuits*, vol. 60, no. 1, pp. 332–346, Jan. 2025.
- [10] Y. Wang et al., “A 28 nm 27.5 TOPS/W approximate-computing-based transformer processor with asymptotic sparsity speculating and out-of-order computing,” in *IEEE Int. Solid-State Circuits Conf. (ISSCC) Dig. Tech. Papers*, pp. 1–3, Feb. 2022.
- [11] F. Tu et al., “16.1 MuITCIM: A 28 nm 2.24 $\mu$ J/token attention-token-bit hybrid sparse digital CIM-based accelerator for multimodal transformers,” in *IEEE Int. Solid-State Circuits Conf. (ISSCC) Dig. Tech. Papers*, pp. 248–250, Feb. 2023.
- [12] S. Liu et al., “16.2 A 28 nm 53.8 TOPS/W 8b sparse transformer accelerator with in-memory butterfly zero skipper for unstructured pruned NN and CIM-based local-attention-reusable engine,” in *IEEE Int. Solid-State Circuits Conf. (ISSCC) Dig. Tech. Papers*, pp. 250–252, Feb. 2023.
- [13] Stillmaker et al., “Scaling Equations for the Accurate Prediction of CMOS Device Performance from 180nm to 7nm.” *Integration the VLSI Journal*, vol. 5, pp. 74–81, Jan. 2017.